Non-destructive Testing of Cylindrical Ferromagnetic and Non-magnetic Materials Using Eddy Current Tomography

Jacek Salach

Institute of Metrology and Biomedical Engineering Warsaw University of Technology
A. Boboli 8 Str., 02-739 Warsaw, Poland
j.salach@mchtr.pw.edu.pl

Abstract. Idea of the high-resolution eddy current tomography is presented. Proposed system gives possibility of cylinder-shaped elements made of both magnetic and non-magnetic materials testing. To validate the concept, the tomographic measurements were carried out on set of steel cylinders with non-magnetic copper inclusion. Measurements were done during both linear and rotational movement of the element. Achieved results indicate the high sensitivity of system, which creates possibility of its application for non-destructive testing of the elements made of ferromagnetic and non-magnetic materials.

Keywords: Eddy current tomography, non-destructive testing, testing of ferromagnetic materials, testing of non-ferromagnetic materials.

1 Introduction

Tomography based tests are intensively developed for non-destructive testing of mechanical components. The main advantage of tomography is unique possibility of obtaining detailed information about the nature and shape of discontinuities in the tested element. However, commonly used X-ray tomography creates a number of risks typical for X-ray techniques. As a result, this technique is expensive and difficult to use in industrial environment. An alternative to the use of X-ray tomography can be eddy current tomography [3]. It allows for simultaneous measurement of magnetic susceptibility and resistivity of the material [4] in the tested element. Consequently, eddy current tomography opens completely new possibilities for detection of discontinuities in structures in industrial conditions.

There are two steps during eddy current tomography imaging [5]. First, influence of tested element on the coupling of two coils is measured during the movement of element. Next, the shape of the element together with its internal structure is recalculated with the use of finite element method, on the base Maxwell equations [6].

Different methods of inverse eddy current tomography transformation were previously presented [7–9]. However, it seems that development of eddy current tomography setup with high spatial resolution and high accuracy of measurements was not

J. Awrejcewicz et al. (eds.), *Mechatronics: Ideas for Industrial Applications*,
Advances in Intelligent Systems and Computing 317, DOI: 10.1007/978-3-319-10990-9_35

presented previously. This paper is filling this gap, which will enable further development of more effective and accurate algorithms for inverse eddy-current tomography transformation.

2 Tomography Setup

The schematic block diagram of experimental setup is presented in Fig. 1, whereas Fig. 2 presents the model element used for tests.

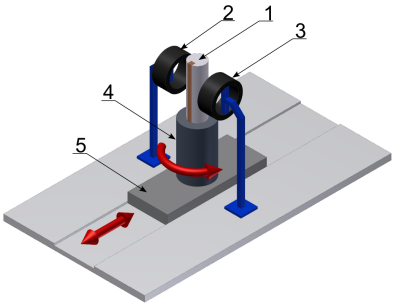

Fig. 1. Schematic block diagram of experimental setup for high resolution eddy current tomography: 1) tested element, 2 – driving coil, 3 – detection coil, 4 – stepper motor for rotation, 5 – linear actuator

Driving coil (2) is connected to sine wave current source. Measuring signal from detection coil (3) consist of both amplitude and phase shift. This signal is filtered by a band-pass filter to decrease noise level. On the base of these data, internal structure of tested element (1), from the point of view of magnetic permeability and conductivity, may be calculated on the base of Maxwell equations.

During the measurement, the test object is rotated by the stepper motor (4). Additionally, after each rotation object is moved incrementally by linear actuator (5). Schematic block diagram of signal processing unit is presented in Fig. 3.

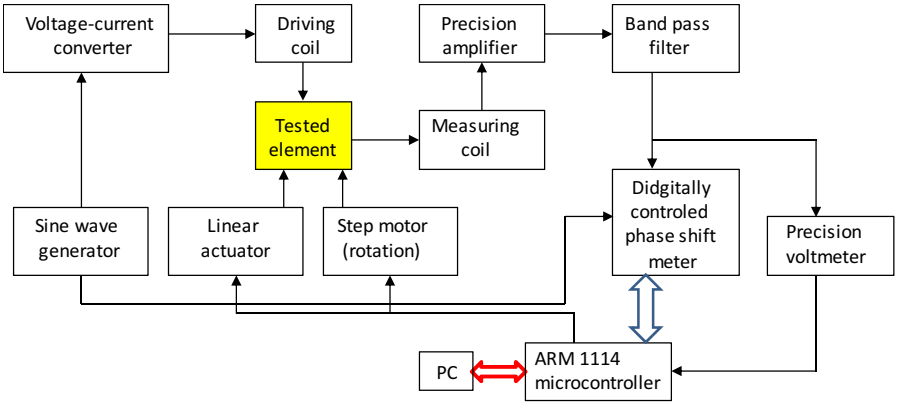

Fig. 2. Schematic block diagram of electronic signal processing unit in eddy-current tomography

Exciting coil is powered by a current sine wave with 2 kHz frequency, generated by a sinusoidal voltage generator circuit using ICL8038 integrated circuit and voltage-to-current converter with large output current. Signal from detection coil is amplified and the first harmonic (2 kHz) is filtered. From practical point of view, other harmonics are negligible due to the fact, that magnetization process for lower magnetizing field is connected with bending of magnetic domain walls. As a result it is nearly linear.

After filtering, the electronic measuring system provides a measurement of both the amplitude of the signal obtained in the detection coil and the angle of the phase shift with respect to the magnetizing coil driving signal. Phase shift is measured as a tangent of the shift between the driving coil signal and detected signal. All measuring data are collected by ARM1114 microcontroller produced by NXP. This microcontroller also controls both linear and rotation actuators as well as provides measuring data to PC for further processing.

For determination of spatial distribution of both magnetic permeability μ and resistivity ρ finite element method can be applied [10–12]. This method utilizes fundamental Maxwell equations written in frequency domain [5, 6]:

$$\nabla \times E = -j\omega B \tag{1}$$

$$\nabla \times H = E/\rho + j\omega\varepsilon E \tag{2}$$

$$\nabla \cdot (E/\rho) = 0 \tag{3}$$

Moreover, for frequencies up to 10 kHz, electromagnetic coupling may be neglected. As a result, both spatial distribution of magnetic permeability μ and resistivity ρ in the tested element may be calculated on the base of solution of partial differential equations, as it was presented before [11, 12].

3 Results of Investigation

Experiment was carried out for three cylinders made of S235 JR construction steel. In each cylinder copper block inclusion was made. The inclusion block was inserted 13 mm into the cylinder, whereas its wideness was 4 mm, 8 mm and 12 mm respectively. As it is presented in Fig. 3, the copper block inclusion was made on whole length of model element.

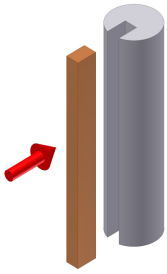

Fig. 3. Model element consisting construction steel S235 JR cylinder with copper inclusion

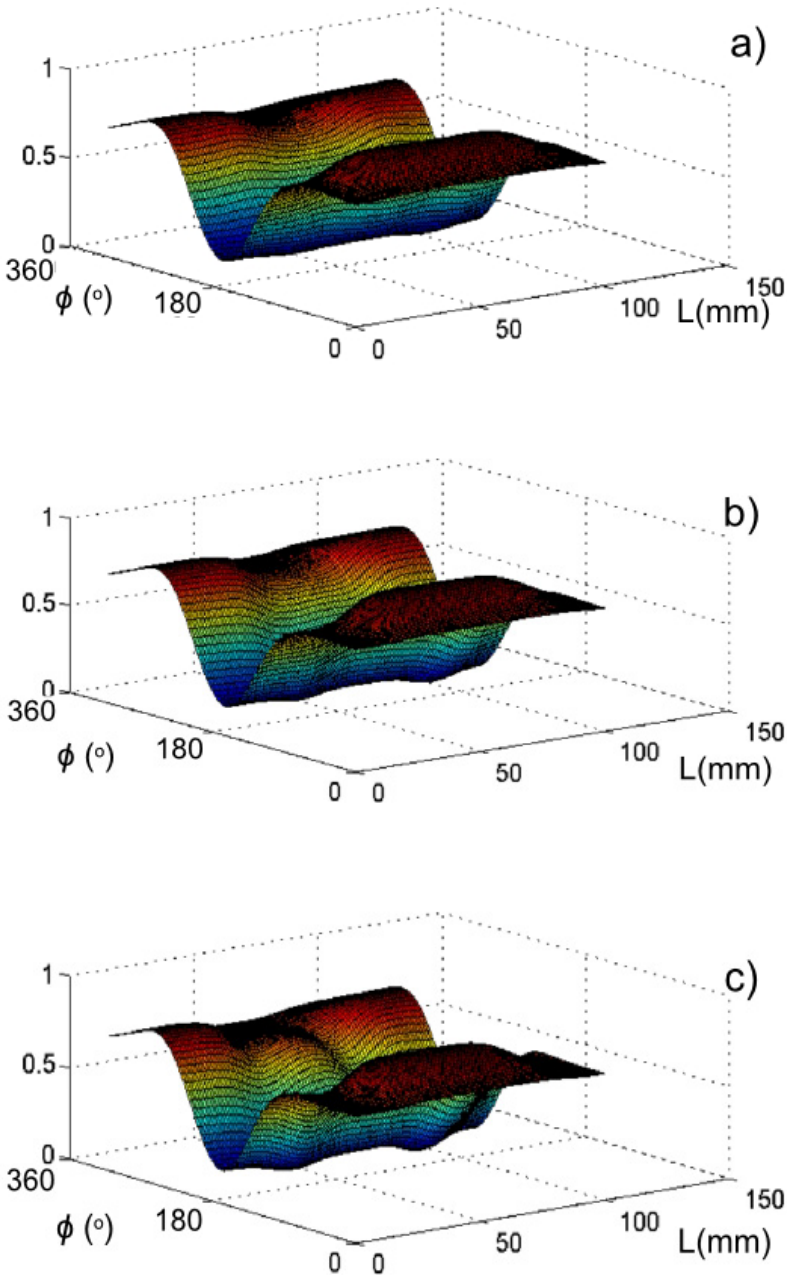

Fig. 4. Visualized results of measurements the volume of amplitude of the signal on detection coil as a function of linear movement L and rotation ϕ for model steel elements with copper inclusions width: a) 4 mm, b) 8 mm, c) 12 mm

The results of measurements of amplitude on the detection coil for all three testing elements are presented in Fig. 4, while the results of measurements of the tangent of angle between signal on measuring coil and signal given on driving coil are shown in Fig. 5. Figures show the changes of amplitude value and of tangent of the angle between signals, as a function of the rotation and linear movement of the test element.

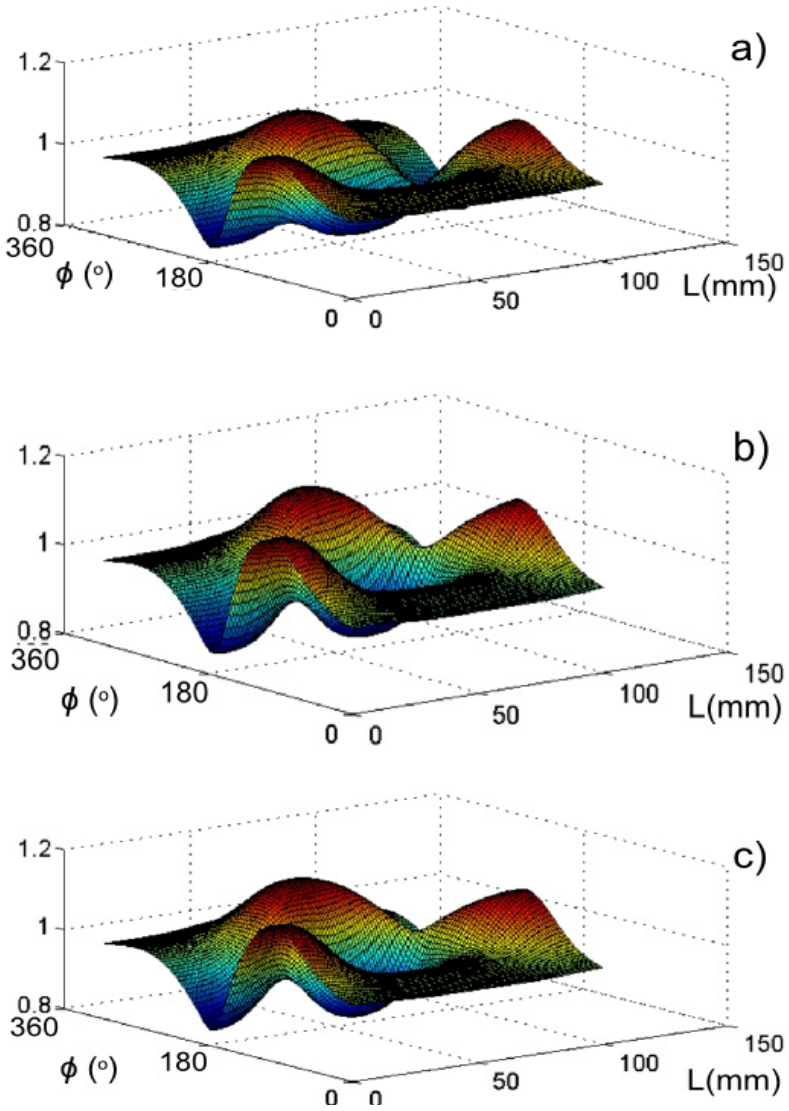

Fig. 5. Visualized results of measurements the volume of tangent of angle between signal on measuring coil and signal given on driving coil as a function of linear movement L and rotation ϕ for model steel elements with copper inclusions width: a) 4 mm, b) 8 mm, c) 12 mm

During the tests the repeatability of measurements was verified. Standard deviation of measurements in point doesn't exceed 1 %. Such high repeatability is very important from the point of view of accuracy of the results of further inverse tomographic transform.

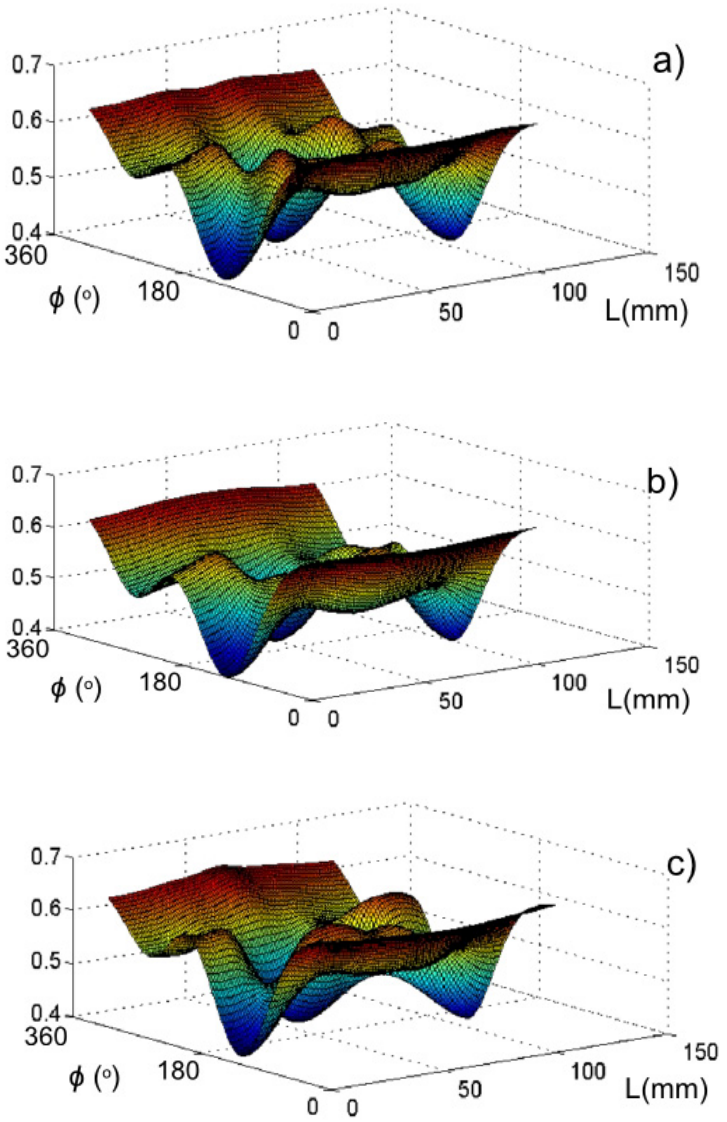

Fig. 6. Results of measurements of amplitude of the signal on detection coil as a function of linear movement L of the element and its rotation ϕ for copper rod elements with different width of steel inclusions: a) 4 mm, b) 8 mm, c) 12 mm

Results of similar measurements of amplitude and tangent of angle between signal on measuring coil and signal given on driving coil, carried out in the same conditions, but for copper rod elements with diversified steel inclusions are presented in figures 6 and 7 respectively.

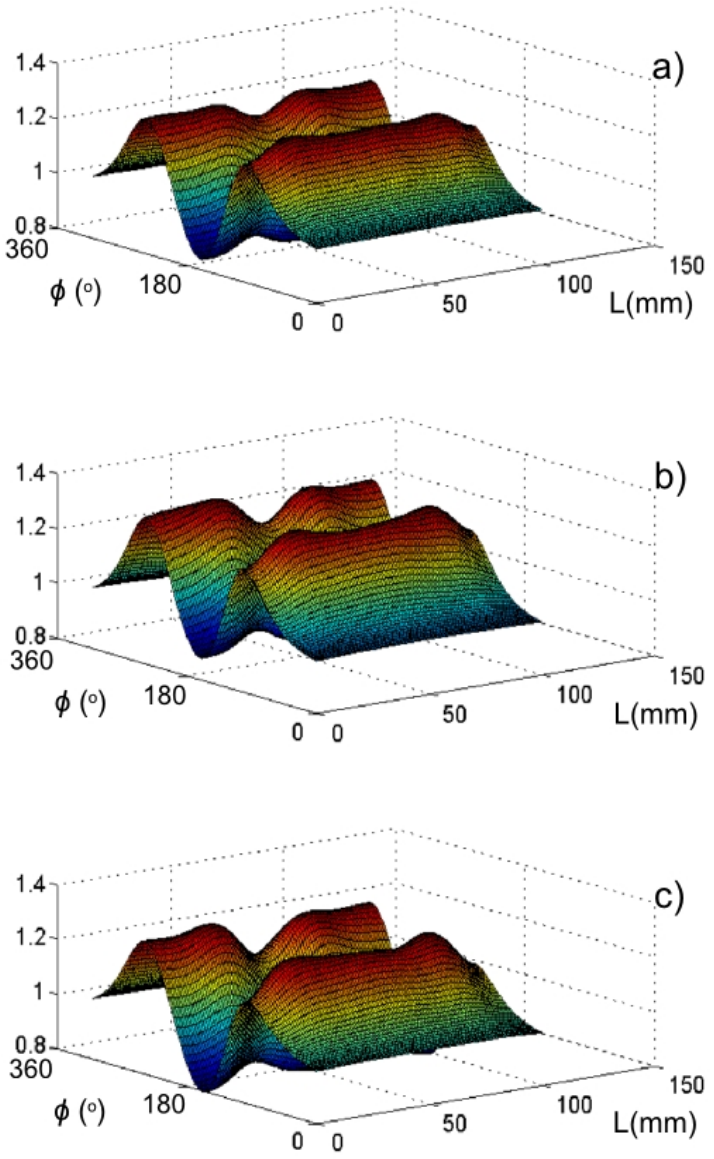

Fig. 7. Results of measurements of tangent of angle between signal on measuring coil and signal given on driving coil as a function of linear movement L of the element and its rotation ϕ for copper rod elements with different width of steel inclusions: a) 4 mm, b) 8 mm, c) 12 mm

4 Conclusions

Eddy current tomography setup presented in the paper creates possibility of tomography measurements with resolution much higher than previously reported [7]. Moreover, obtained results confirm possibility of non-magnetic inclusion in ferromagnetic cylindrical elements assessment. Value of amplitude in sensing coil changes up to 60 % during the measurements and up to 400 % for measurements of similar steel rods. Tangent of angle between signal on measuring coil and signal given on driving coil for test elements described above changed about 40 % and 60 % respectively. Repeatability of these measurements was measured by standard deviation of indication. It was about 1 % for both amplitude and tangent of angle between signal on measuring coil and signal given on driving coil.

The results presented in the paper confirm, that presented eddy current tomography setup is suitable for non-destructive testing of rod-shaped elements. During the tests, the spatial distribution of both permeability μ and resistivity ρ can be determined. It creates the possibility of detection of all types of discontinuities in construction materials, both ferromagnetic and non-magnetic.

References

1. Hsieh, J.: Computed Tomography Principles, Design, Artifacts, and Recent Advances. Wiley (2009)
2. Tamburrino, A., Rubinacci, G.: Fast methods for quantitative eddy-current tomography of conductive materials. IEEE Trans. Mag. 42(8), 2017–2028 (2006)
3. Premel, D., Mohammad-Djafari, A.: Eddy current tomography in cylindrical geometry. IEEE Trans. Mag. 31(3), 2000–2003 (1995)
4. Soleimani, M.: Simultaneous reconstruction of permeability and conductivity in magnetic induction tomography. J Electromagnet Wave 23, 785–798 (2009)
5. Soleimani, M., Tamburrino, A.: Shape reconstruction in magnetic induction tomography using multifrequency data. Int. J. Inform. Sys. Scien. 2, 343–347 (2006)
6. Ioan, D., Rebican, M.: Numerical Model for Eddy-Current Testing of Ferromagnetic Steel Parts. IEEE Trans. Mag. 38, 629–633 (2002)
7. Zhao, Q., Chen, G., Hao, J., Xu, K., Yin, W.: Numerical approach for the sensitivity of a high-frequency magnetic induction tomography system based on boundary elements and perturbation method. Meas. Sci. Technol. 24, 40–44 (2013)
8. Ke, L.: An Improved Back-Projection Algorithm for Magnetic Induction Tomography Image Reconstruction. Adv. Mater. Res. 647, 630–635 (2013)
9. Ke, L., Pang, P.-P., Du, Q.: Forward problem simulation in magnetic induction tomography based on galerkin finite element method. Chines. J. Biomed. Eng. 31(1), 53–58 (2012)
10. Wang, X., Lv, Y., Chen, Y.-Y., Jin, J.-J., Yang, D.: Simulation of forward problem for 3D eddy current in magnetic induction tomography. J. Sys. Sim. 24(4), 780–788 (2012)
11. Kai, X., Cao, Z., Mi, W., Yin, W.: A fast eddy current forward solver for EMT based on finite element method (FEM) and negligibly coupled field approximation. In: Proceedings of the IEEE Int. Conf. Imag. Sys. Tech., IST 2011, pp. 16–20 (2011)
12. Li, Q., Bai, T., Zhu, C.: Deicing excitation simulation and structural dynamic analysis of the electro-impulse deicing system. Appl. Mech. Mater. 66-68, 390–395 (2011)